**Author Contributions:**

**Conceptualization:** Anton Orlov, Steven De Hertog, Felix Havermann, Suqi Guo, Iris Manola, Wim Thiery, Quentin Lejeune, Julia Pongratz, Florian Humpenöder, Michael Windisch, Shruti Nath, Carl-Friedrich Schleussner
**Formal analysis:** Anton Orlov
**Visualization:** Anton Orlov, Steven De Hertog
**Writing – original draft:** Anton Orlov, Steven De Hertog, Felix Havermann, Suqi Guo, Iris Manola, Wim Thiery, Quentin Lejeune, Julia Pongratz, Florian Humpenöder, Michael Windisch, Shruti Nath, Alexander Popp, Carl-Friedrich Schleussner

# Changes in Land Cover and Management Affect Heat Stress and Labor Capacity

Anton Orlov[1], Steven De Hertog[2], Felix Havermann[3], Suqi Guo[3], Fei Luo[4,5], Iris Manola[4], Wim Thiery[2], Quentin Lejeune[6], Julia Pongratz[3,7], Florian Humpenöder[6], Michael Windisch[8,9], Shruti Nath[6], Alexander Popp[8], and Carl-Friedrich Schleussner[6]

[1]Center for International Climate Research, Oslo, Norway, [2]Department of Hydrology and Hydraulic Engineering, Vrije Universiteit Brussel, Brussels, Belgium, [3]Department of Geography, Ludwig Maximilian University Munich, Munich, Germany, [4]Institute for Environmental studies, Vrije Universiteit Amsterdam, Amsterdam, The Netherlands, [5]Royal Netherlands Meteorological Institute (KNMI), De Bilt, The Netherlands, [6]Climate Analytics, Berlin, Germany, [7]Max Planck Institute for Meteorology, Hamburg, Germany, [8]Potsdam Institute for Climate Impact Research, Potsdam, Germany, [9]Institute for Atmospheric and Climate Science, ETH Zurich, Zurich, Switzerland

**Abstract** Global warming is expected to exacerbate heat stress. Additionally, biogeophysical effects of land cover and land management changes (LCLMC) could substantially alter temperature and relative humidity locally and non-locally. Thereby, LCLMC could affect the occupational capacity to safely perform physical work under hot environments (labor capacity). However, these effects have never been quantified globally using a multi-model setup. Building on results from stylized sensitivity experiments of (a) cropland expansion, (b) irrigation expansion, and (c) afforestation conducted by three fully coupled Earth System Models (ESMs), we assess the local as well as non-local effects on heat stress and labor capacity. We found that LCLMC leads to substantial changes in temperature; however, the concomitant changes in humidity could largely diminish the combined impact on moist heat. Moreover, cropland expansion and afforestation cause inconsistent responses of day- and night-time temperature, which has strong implications for labor capacity. Across the ESMs, the results are mixed in terms of sign and magnitude. Overall, LCLMC result in non-negligible impacts on heat stress and labor capacity in low-latitude regions during the warmest seasons. In some locations, the changes of monthly average labor capacity, which are induced by the local effects of individual LCLMC options, could reach −14 and +15 percentage points. Thus, LCLMC-induced impacts on heat stress and their consequences for adaptation should be accounted for when designing LCLMC-related policies to ensure sustainable development.

**Plain Language Summary** Global warming is expected to exacerbate heat stress. Changes in land cover and land management (LCLMC) alter temperature and humidity locally and remotely, thereby potentially affecting the occupational capacity to safely perform physical work under hot environments (labor capacity). The effects of LCLMC on labor capacity have not been quantified globally using multiple climate models. Here, we assessed the effects of cropland expansion, irrigation expansion, and afforestation on heat stress and labor capacity using a multi-model approach. We found that LCLMC leads to substantial changes of temperature, but the concomitant changes of humidity could largely diminish the combined effects on moist heat. Temperature changes in response to cropland expansion and afforestation differ between day- and night-time and are inconsistent across the climate models. Overall, LCLMC leads to non-negligible impacts on heat stress and labor capacity in low-latitude regions during the warmest seasons. LCLMC-induced impacts on heat stress and their consequences for adaptation should be accounted for when designing LCLMC-related policies to ensure sustainable development.

## 1. Introduction

Increasing evidence reveals that land cover and land management change (LCLMC) can have a substantial impact on climate through the biogeophysical effects resulting from modifications of the radiative, aerodynamic and thermodynamic properties of the land surface (Chen & Dirmeyer, 2019; De Hertog et al., 2023; de Vrese et al., 2016; Pongratz et al., 2021; Thiery et al., 2017). Biogeophysical effects can be local and non-local. The local effects are potential climatic changes in a region where LCLMC is implemented, whereas the non-local effects are associated with changes in atmospheric circulation caused by LCLMC implemented in outermost regions. For irrigation, it was found that irrigation has significantly reduced the exposure to heat extremes in the

**Writing – review & editing:** Anton Orlov, Steven De Hertog, Felix Havermann, Suqi Guo, Iris Manola, Wim Thiery, Quentin Lejeune, Julia Pongratz, Florian Humpenöder, Michael Windisch, Shruti Nath, Alexander Popp, Carl-Friedrich Schleussner

past (Chen & Dirmeyer, 2019; Thiery et al., 2017, 2020). Furthermore, irrigation could also have a significant non-local effect on the climate by remotely affecting temperature and precipitation in other regions (de Vrese et al., 2016). However, there are still big uncertainties about the magnitude and spatial patterns of local and non-local effects of irrigation. Moreover, the combined effect of irrigation-induced temperature and humidity changes on moist heat is not well understood. For instance, in a case study for India, it was found that irrigation could increase the moist heat because of a higher humidity (Guo et al., 2022; Krakauer et al., 2020; Mishra et al., 2020). For deforestation and afforestation, temperature changes induced by forest cover changes could be several degrees in some regions; however, the magnitude and spatial patterns of local and non-local biogeophysical effects on climate are also highly uncertain (Boysen et al., 2020; Winckler et al., 2019). Results from an idealized sensitivity experiment on global deforestation using the model outputs from Phase 6 of the Coupled Model Intercomparison Project (CMIP6) show an increase in temperature in the tropics and cooling over the boreal area (Boysen et al., 2020). A warming due to projected deforestation over the Amazon and Congo basins was also found in several region-focused studies (Akkermans et al., 2014; Baker & Spracklen, 2019; Lejeune et al., 2015).

LCLMC-induced climate effects could indirectly affect economies and societies through different transmission channels. For example, extreme temperatures increase the risk of mortality and morbidity from cardiovascular and respiratory diseases (Gasparrini et al., 2015). Climate-induced sick leaves and occupational injuries reduce working hours (labor capacity) (Fatima et al., 2021). Moreover, extreme temperatures might also limit the ability to work overtime. Apart from labor capacity, heat stress could also reduce labor productivity (Dunne et al., 2013; Kjellstrom et al., 2009). Heat-induced reductions of labor capacity and productivity are found to be substantial, particularly in low-latitude regions, which are typically exposed to the risk of heat stress (Kjellstrom et al., 2018, 2019; Mora et al., 2017). The associated global and regional economic cost could also be considerable under future high warming scenarios, especially when adaptive capacity is limited (Orlov et al., 2020; Takakura et al., 2017). For example, the cost of human heat stress could increase regional cost of crop production by 10% or more in tropical regions (Orlov et al., 2021). Heat stress impacts on labor can also increase poverty in regions with a limited adaptive capacity (Saeed et al., 2022). While several studies investigated the heat stress impacts under different future warming scenarios, relatively little research has been done on quantifying the effects of LCLMC on heat stress, and productivity and capacity of labor. A few related studies show that LCLMC-induced heat stress impacts could be considerable. For example, in a field experiment study for Indonesia, Masuda and colleagues show that labor productivity was 8% lower in deforested area than in afforested area (Masuda et al., 2021). A high risk of heat stress and work capacity loss under high warming scenarios and deforestation was also found in case studies across Brazil (Alves de Oliveira et al., 2021; Parsons et al., 2021). However, currently there is no single global-scale study that investigates the local and non-local effects of LCLMC on economies and society.

The objective of this study is to address this knowledge gap, focusing on heat-induced impacts on labor capacity. Specifically, we investigate the effectiveness of LCLMC as adaptation strategies for reducing heat stress. Our global analysis builds upon the results from stylized global sensitivity experiments for three LCLMC practices (a) cropland expansion, (b) irrigation expansion, and (c) afforestation, which are described and analyzed in (De Hertog et al., 2023). To directly separate between local and non-local effects of LCLMC, the checkerboard approach developed by Winckler et al. (2017a) was applied in these simulations. Following this distinction, the local effects of LCLMC represent the expected local climate consequences in case the same amount and type of LCLMC is applied in any scenario, whereas the non-local effects are those climate consequences occurring elsewhere and depend on the global extent and patterns of LCLMC. The sensitivity experiments were implemented using three Earth System Models (ESMs), which allows to investigate modeling uncertainties. While our impact assessment is based on the idealized sensitivity experiments, the separation into local and non-local effects still provides valuable insights into a potential magnitude of LCLMC-induced impacts on human heat stress and labor capacity.

## 2. Materials and Methods

### 2.1. Earth System Model Simulations

Our analysis is based on the results from three ESMs: the Community Earth System Model (CESM) version 2 (Danabasoglu et al., 2020), the Max Planck Institute Earth System Model (MPI-ESM) version 1.2 (Mauritsen et al., 2019), and the European Community Earth System Model (EC-Earth 3.3.1) (Döscher et al., 2022). Below, we provide a short description of the conducted sensitivity experiments on LCLMC. A detailed description of the model simulations can be found in (De Hertog et al., 2023).
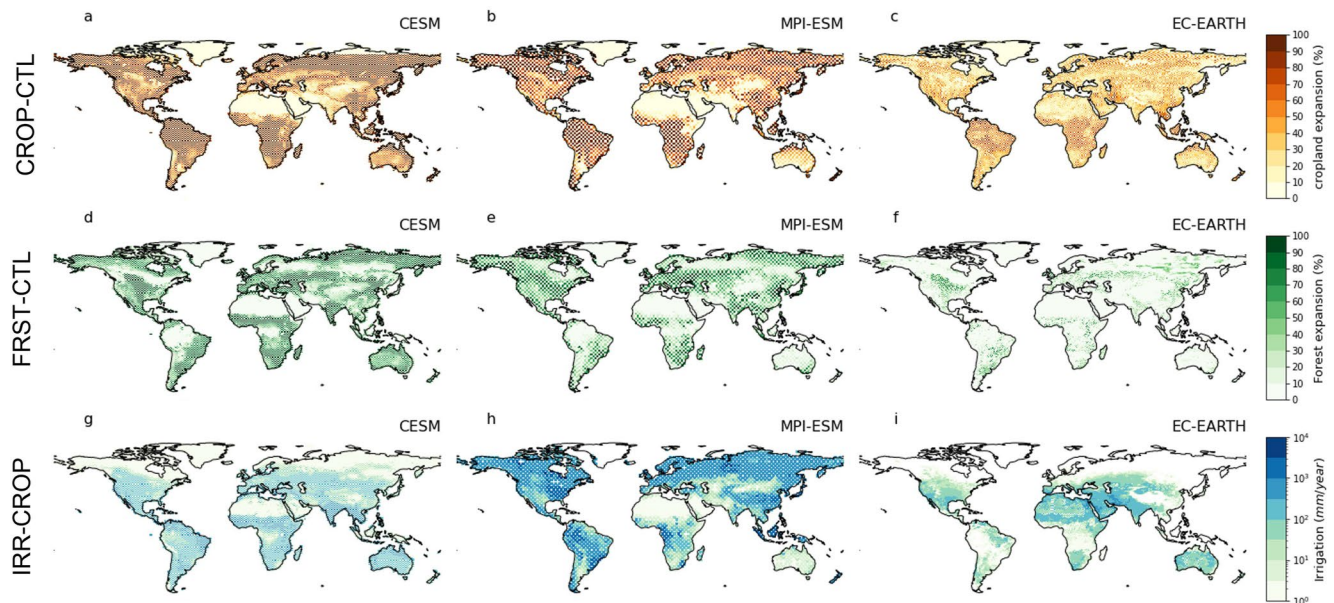
**Figure 1.** LCLMC implemented in the sensitivity experiments. The fraction of cropland expansion simulated in CROP compared to CTL is shown for CESM (a), MPI-ESM (b), and EC-Earth (c). The fraction of afforestation simulated in FRST compared to CTL is show for CESM (d), MIP-ESM (e), and EC-Earth (f). The amount of irrigation simulated in IRR compared to CROP is shown for CESM (g), MPI-ESM (h), and EC-Earth (i). Compared to CESM and MPI-ESM, in EC-Earth, the surface maps are dynamic, so the maximal differences are taken for this ESM. Source: De Hertog et al. (2023).

We use the data simulated by a reference scenario and three sensitivity experiments: (a) cropland expansion (CROP) (a fully deforested world where crops cover all the vegetated area, only rainfed crops), (b) irrigation expansion (IRR) (same as CROP but with an extensive irrigation), (c) afforestation (FRST) (i.e., a fully afforested world) (Figure 1). The reference scenario (i.e., control simulation (CTL)) represents the present-day land cover at the end of year 2014 which is based on Version two of the Land Use Harmonization (LUH2) dataset (Hurtt et al., 2020). Although cropland expansion includes other land cover changes, such as conversion of grass/shrub to cropland, in the tropics, cropland expansion is mostly achieved through deforestation, and other land cover conversion happening in this region (grassland to cropland) does not lead to substantial climate changes via biogeophysical effects (Figure S1 in Supporting Information S1). For cropland expansion, the present crop coverage was upscaled to fill up the grid cells. Crop types differ across the ESMs; CESM has eight different crop types (i.e., temperate soybean, tropical soybean, temperate corn, tropical corn, spring wheat, cotton, rice, and sugarcane), MPI-ESM simulates C3 and C4 crops, and EC-Earth has five crop functional types, both annual and perennial C3 and C4 crops, and C3 N fixers (Lindeskog et al., 2013). Also, the growth periods differ by crop type and ESM. For irrigation expansion, CESM has a distinct seasonality for irrigation, and irrigation is turned when there is water stress. In EC-Earth, irrigation is prognostically determined depending on the plant water deficiency. MPI-ESM simulates irrigation to the soil layer directly if soil moisture content is below field capacity. Irrigation water is taken from an irrigation reservoir which is filled by runoff and drainage until a defined threshold value.

### 2.2. Local and Nonlocal Effects Decomposition

The LCLMC of cropland expansion, irrigation expansion, and afforestation are implemented in the ESMs only for half of all grid cells in a regular checkerboard pattern, which allows explicitly distinguishing between their local and non-local effects using the approach developed by Winckler et al. (2017a). The local effects represent the local climate changes where LCLMC are applied, while the non-local effects are shared with neighboring or remote areas. Importantly, the local effects should be interpreted as potential local changes over one grid cell and independent of how LCLMC is implemented elsewhere, whereas the non-local effects will vary depending on the extent and pattern of global LCLMC. While the local effects could be affected by changes in the background climate due to the non-local effects through the interaction between surface conditions, boundary layer dynamics and free atmosphere, Winckler et al. (2017a) found that the local effects are robust for changes in the background climate due to the non-local effects.

The differences in climate responses between CROP and CTL simulations (CROP-CTL) show the effects of cropland expansion; IRR-CROP shows the effects of irrigation expansion in a cropland world; and FRST-CTL quantifies the climate response to full afforestation starting from present-day conditions. In EC-Earth, irrigation does not induce any local effects on climate because irrigation implemented in the process-based vegetation model, LPJ-GUESS, does not affect moisture fluxes in the atmosphere due to disconnected water cycles of the land surface model interface to the atmospheric boundary layer (De Hertog et al., 2023). Therefore, for the sensitivity experiment of irrigation expansion, we only discuss results of CESM and MPI-ESM simulations. All simulations are conducted given the assumption of a constant anthropogenic forcing (i.e., greenhouse gases [GHG] and aerosol concentration) at 2015 levels. The simulations run over 160 years, of which 10 years are considered as spin-up, and the remaining 150 years are divided into five 30-year time slices (ensemble members). The ensemble mean is used to investigate the average climate responses when averaging out internal climate variability, whereas the individual 30-year time slices are used to assess the robustness of the results by investigating their consistency across all time slices.

## 2.3. Heat Stress Metrics

Thermal comfort and heat stress are determined by many climatic factors, such as temperature, humidity, wind speed, and radiation (Parsons, 2014). Several heat indexes were developed to quantify the compound effect of climatic conditions on occupational health (Lemke & Kjellstrom, 2012). The most widely used heat index to assess heat stress impacts on capacity and productivity of labor is the Wet Bulb Globe Temperature (WBGT) index (Budd, 2008). In our analysis, we use the WBGT to assess the effects of LCLMC on moist heat. For indoor work environments (in shade, shielded from direct solar radiation), the WBGT-indoors is calculated as a weighted average of wet bulb temperature (WBT) and temperature (Equation 1) (Lemke & Kjellstrom, 2012). WBT is calculated using temperature and relative humidity (or dew point temperature), applying the Stull formula (Stull, 2011) (Equation 2).

$$\text{WBGT}_{\text{indoors}} = 0.67 * \text{WBT}_{\text{stull}} + 0.33 * tas \tag{1}$$

$$\begin{aligned} \text{WBT}_{\text{stull}} = tas * \text{atan}(c1 * \sqrt{hurs + c2}) + \text{atan}(tas + hus) - \text{atan}(hurs - c3) \\ + c4 * \left(hurs^{\frac{3}{2}}\right) * \text{atan}(c5 * hurs) - c6 \end{aligned} \tag{2}$$

$$ESI = 0.63 * tas - 0.03 * hurs + 0.002 * rsds + 0.0054 * tas * hurs - \left(\frac{0.073}{0.1 + rsds}\right)$$

where $tas$ is the near-surface air temperature in Celsius, $hurs$ is the near-surface relative humidity in percentages, atan is the inverse tangent of a number, $c1$, $c2$, $c3$, $c4$, $c5$, and $c6$ are the constant coefficients in Stull formula.

For outdoor work environments (in the sun), the calculation of WBGT-outdoors also requires the data on solar shortwave downwelling radiation as solar radiation causes an additional heat stress impact. Some sophisticated approaches to calculate the WBGT-outdoors also include wind speed (Liljegren et al., 2008). There are different methods to calculate the WBGT; some are based on thermodynamic heat exchange mechanisms, and others are based on statistical models' calculations (Lemke & Kjellstrom, 2012). A simplified method for WBGT-outdoors is widely used in climate literature (Buzan et al., 2015; Fischer & Knutti, 2013; Willett & Sherwood, 2012). However, some validation studies found that this method could largely overestimates the response of moist heat at the mean level but underestimate the extreme heat stress particularly under strong radiation and calm wind (Kong & Huber, 2022; Lemke & Kjellstrom, 2012). More accurate and sophisticated methods to calculate WBGT-outdoors require iterative solutions, which are computationally intensive. In our analysis, for outdoor work environments, we use the Environmental Stress Index (ESI) as a substitute for the WBGT-outdoors (Equation 3).

$$ESI = 0.63 * tas - 0.03 * hurs + 0.002 * rsds + 0.0054 * tas * hurs - \left(\frac{0.073}{0.1 + rsds}\right) \tag{3}$$

where $rsds$ is the shortwave downwelling solar radiation in Watt per $m^2$.

Both metrics are found to be highly correlated, while the computation of ESI requires less climate variables, and is computationally less intensive while preserving satisfactory accuracy (Moran & Epstein, 2006; Moran et al., 2001). Kong and Huber (2022) found that ESI, although subject to biases in representing severe heat stress, performs reasonably well in representing mean-level heat stress and the integrated impact over a long period (i.e., seasonal labor capacity). Using the sub-daily data on the near-surface temperature, relative humidity, and solar

**Table 1**
*Recommended Rest/Work Ratios for ESI Exposure Levels (°C) for an Average Acclimatized Worker Wearing Light Clothing, for High Work Intensive Jobs Outdoors With a Metabolic Rate of 400 W*

| Rest/work ratios | WBGT-indoors/ESI (°C) |
| --- | --- |
| 0% rest/hour (continuous work) | 27 |
| 25% rest/hour | 27.5 |
| 50% rest/hour | 29.5 |
| 75% rest/hour | 31.5 |
| 100% rest/hour (no work) | 36 |

Source: Kjellstrom et al. (2009).

radiation, we calculate the WBGT-indoors and ESI for four simulations CTL, CROP, IRR, and FRST conducted by the three ESMs.

### 2.4. Impacts on Labor Capacity

To quantify the heat-induced impacts on labor capacity, we apply the widely used heat assessment metric based on the National Institute for Occupational Safety and Health (NIOSH) standards (Kjellstrom et al., 2009; NIOSH, 1986). Labor capacity is defined as the occupational capacity to safely perform physical work under heat stress (Dunne et al., 2013). The NIOSH standards describe the frequency and duration of rest breaks, which are recommended to avoid heat-induced illnesses, for different metabolic rates (i.e., levels of work intensity). The recommended heat stress exposure limits apply for a "standard" acclimatized worker of 70 kg. Labor capacity is quantified as the percentage of a working hour that a worker performs (i.e., rest/work ratios) (Table 1). For example, if no rest break due to heat stress is needed, then the labor capacity is 100%, and if a 25% rest break at work is needed to prevent heat-related health risk, then the labor capacity is 75% of total working hours (Kjellstrom et al., 2009). The recommended rest/work ratios presented in Table 1 are linearly interpolated for different levels of WBGT-indoors/ESI.

Work intensity is an important vulnerability factor determining heat stress because physical work increases the metabolic heat in the body. As we primarily focus on the sectors which are mostly exposed to heat stress, we quantify the heat-induced impacts on labor capacity for high-intensity jobs (e.g., agriculture and construction). The levels of labor capacity are calculated using WBGT-indoors and ESI at the native spatial and temporal (sub-daily) resolution of the ESMs. Then, we calculate the multi-year monthly and sub-daily mean values of labor capacity over multiple years for each 30-year time slice. For CESM and EC-Earth, the temporal resolution is 3-hourly and for MPI-ESM, it is 6-hourly. Finally, the local and non-local components of LCLMC-induced impacts on moist heat stress (WBGT-indoors/ESI) and labor capacity are disentangled using the checkerboard approach developed by Winckler et al. (2017a). The signal-separated monthly sub-daily responses of ESI and labor capacity are linearly interpolated to hourly and then converted from Universal Time Coordinated (UTC) to local time. To analyze the annual and seasonal average responses of ESI and labor capacity, we calculate the mean values of a 12-hr workday from 7 a.m. to 7 p.m. This time range aims to include the core work hours across all regions. The robustness of the results for each ESM is indicated by the consistency in terms of the sign of the effects across five 30-year time slices. Although we computed the labor responses for indoor (using WBGT-indoors) and outdoor work (using ESI) environment, below we present the results for outdoor work, which is more exposed to heat stress. Overall, we found that the labor responses under these two heat indexes are similar but more pronounced when using ESI.

## 3. Results

### 3.1. Local Effects

#### 3.1.1. Cropland Expansion

In CESM, the local effects of cropland expansion result in an increase of annual average near-surface air temperature (hereafter: temperature) in the tropics due to decreased evapotranspiration rates, whereas the boreal regions experience an albedo-induced cooling (De Hertog et al., 2023) (Figure S2 in Supporting Information S1). For low latitudes, the absolute increase of ESI is less pronounced than the temperature increase, because of a reduction in (relative and specific) humidity. CESM also shows a small reduction in specific humidity in low latitudes and an increase in shortwave solar radiation in particular in high latitudes. There are substantial differences in the seasonal and especially sub-daily responses of ESI. For example, for East Asia (mostly China), the local effects of cropland expansion cause an ESI warming mostly in fall and winter, while in summer, the local warming effect is modest (Figure 2). The seasonal difference likely occurs because of the Asian summer monsoon, which causes more evaporation due to more ample water and thus weaken the warming in summer. Regarding the diurnal cycle, the local effects of cropland expansion lead to a higher (lower) ESI in the night-time (day-time) in the tropics (Figure 3). In CESM, day-time temperature is mostly only affected in high northern latitudes, whereas during night-time many other regions are affected as well. Despite an increase in temperature and solar radiation, a reduction in humidity leads to a small ESI cooling during day-time in low latitudes (Figure S3 in Supporting Information S1). Overall,
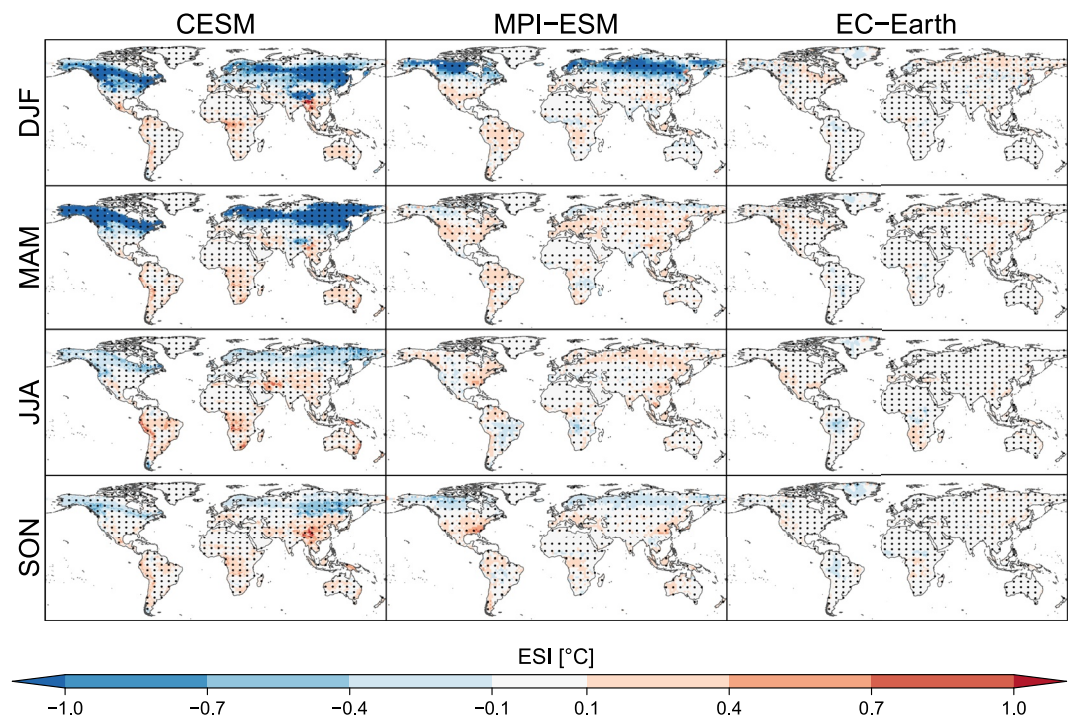
**Figure 2.** Ensemble-mean absolute changes (in Celsius) of seasonal average Environmental Stress Index (ESI) for a 7 a.m. to 7 p.m. workday, which result from the local effects of cropland expansion. The dots indicate the consistency in terms of the sign of local effects across five 30-year time slices.

cropland expansion induces a local increase of seasonal average ESI in low latitudes. However, due to non-linearities of labor responses, a reduction of day-time ESI results in a higher seasonal average capacity of outdoor labor in the Amazon and Congo regions (Figure 4 and Figure S6 in Supporting Information S1). In contrast, in Australia (in DJF) and Iran (in JJA), the local effects of cropland expansion result in a lower capacity of outdoor labor. For South-East Asia countries, such as Myanmar, Thailand, Cambodia, and Indonesia, the results are mixed.

In MPI-ESM, the local effects of cropland expansion lead to a less pronounced and less widespread local cooling in the boreal forest regions and less local warming in the tropics compared to CESM (Figure S2 in Supporting Information S1). This is because the albedo-induced effects in MPI-ESM are weaker than in CESM (De Hertog et al., 2023) Similar to CESM, in MPI-ESM, cropland expansion results in an increase in shortwave solar radiation (Figure S2 in Supporting Information S1). MPI-ESM shows different seasonal patterns in the responses of ESI. For example, the local effects of cropland expansion result in a reduction of ESI in the Amazon region in JJA, while there is an ESI warming in DJF (Figure 2). Furthermore, MPI-ESM shows a different sub-daily response of ESI compared to CESM. In MPI-ESM, cropland expansion causes a local ESI cooling the first half of the day in the Amazon and Congo regions, while afternoon, the local effect is dominated by an ESI warming (Figure 3). In MPI-ESM, the diurnal variation of ESI is largely consistent with the diurnal variation of temperature, while changes in humidity are relatively small (Figure S4 in Supporting Information S1). The impacts on the capacity of outdoor labor are mixed across regions and seasons (Figure 4 and Figure S6 in Supporting Information S1). Similar to CESM, in MPI-ESM, the local effects of cropland expansion in Africa causes an increase in the seasonal average capacity of outdoor labor, especially in SON. In contrast to CESM, the seasonal average capacity of outdoor labor also increases in the Northern Australia in SON and DJF due to less moist heat. The Amazon region (in DFJ and MAM), South-East USA (in JJA), and South-East Asia (in JJA) experience a reduction in the seasonal average capacity of outdoor labor because of an ESI warming.

EC-Earth, compared to CESM and MPI-ESM, does not show any significant local cooling in the boreal regions (Figures S2 in Supporting Information S1), which is likely because of a weak albedo response and a strong local warming over the permafrost areas in this model (De Hertog et al., 2023). Yet, in line with CESM and MPI-ESM, the local effects of cropland expansion induce a moderate local warming effect in the tropics due to decreased evapotranspiration (De Hertog et al. (2023)). The increase of ESI in the tropics is substantially less pronounced
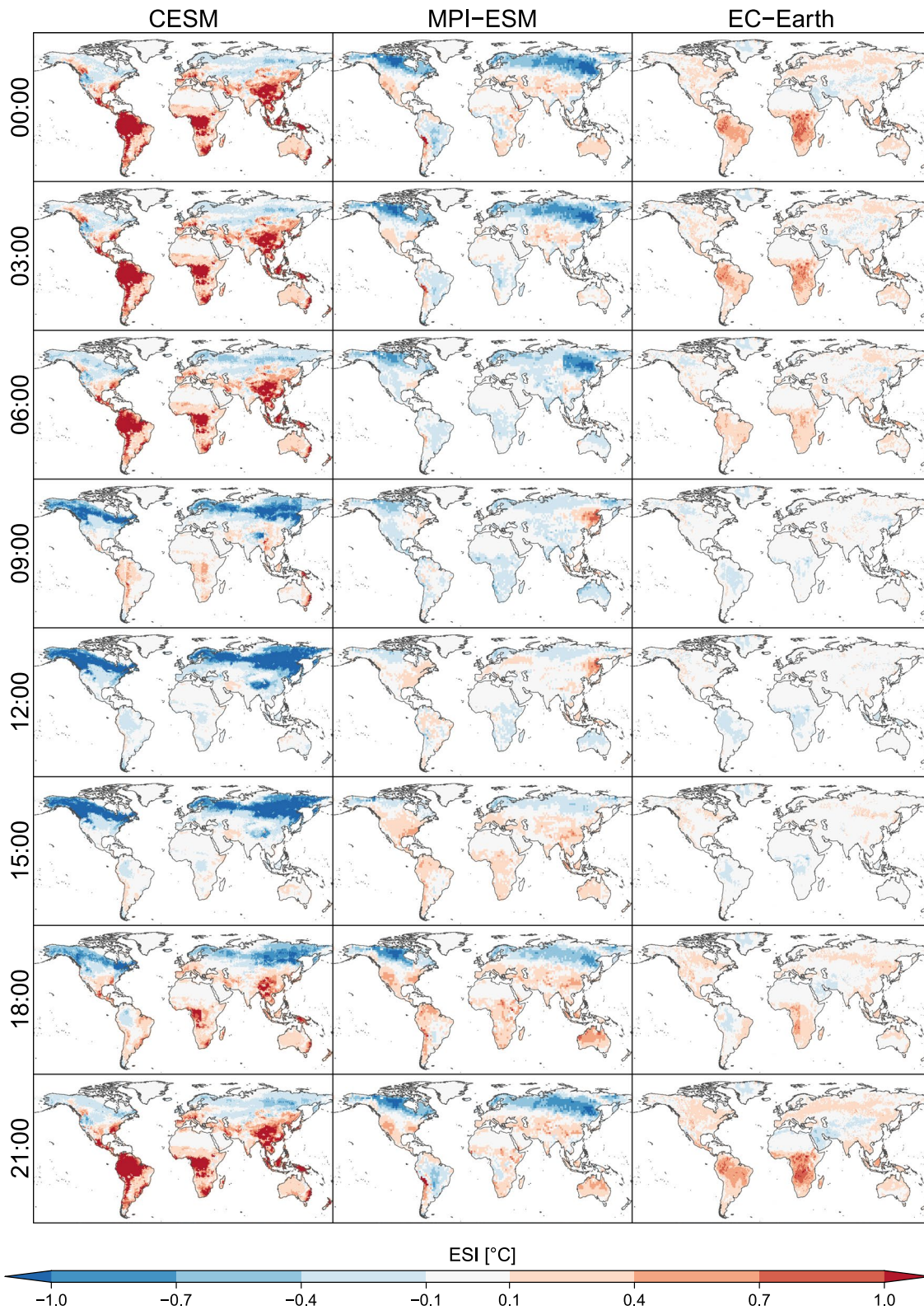
**Figure 3.** Ensemble-mean absolute changes (in Celsius) of sub-daily (local time) average Environmental Stress Index (ESI), which result from the local effects of cropland expansion.
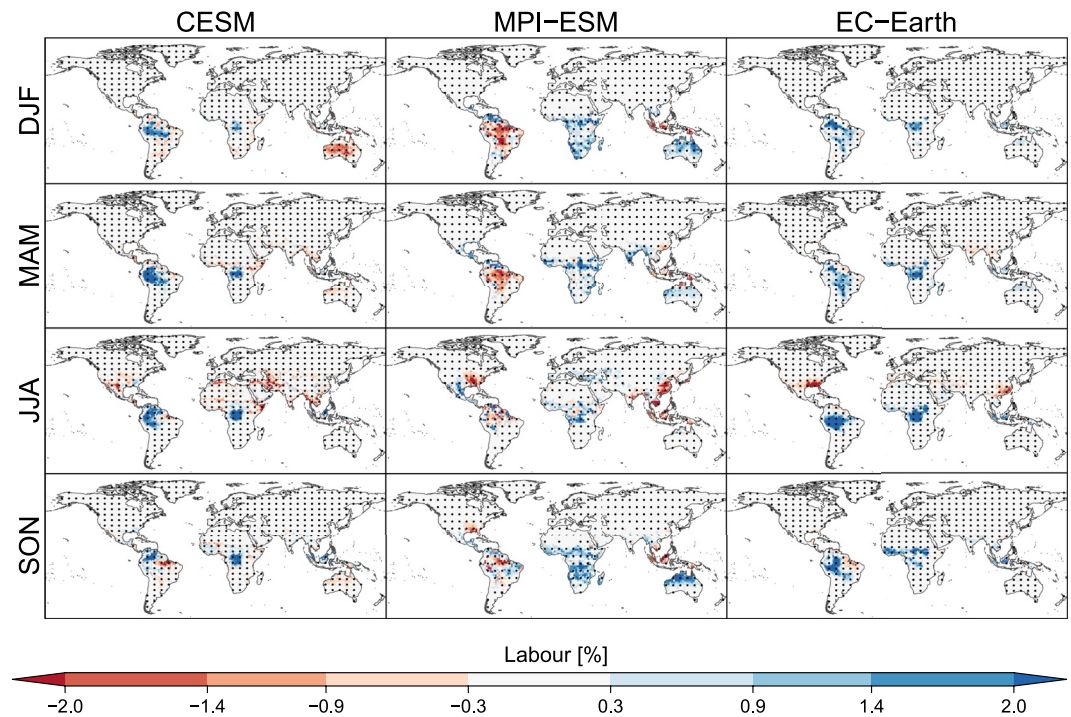
**Figure 4.** Ensemble-mean absolute changes (in percentage points) of the seasonal average labor capacity of high work-intensive jobs in outdoors for a 7 a.m. to 7 p.m. workday, which result from the local effects of cropland expansion. The dots indicate the consistency in terms of the sign of local effects across five 30-year time slices.

than the temperature response because of decreased humidity (Figure S2 in Supporting Information S1). Thus, the changes of seasonal average ESI are also moderate in EC-Earth (Figure 2). Similar to CESM, in EC-Earth, cropland expansion in low latitudes leads to a smaller increase in temperature in day-time compared to night-time. Moreover, the day-time temperature increase is turned into a day-time ESI cooling due to a reduction in humidity (Figure S5 in Supporting Information S1). So, cropland expansion leads to a local increase (decrease) in the night-time (day-time) ESI (Figure 3). Because of non-linearities in labor response functions, the reduction of day-time ESI results in an increase in the seasonal average capacity of outdoor labor in the Amazon and Congo regions, especially in JJA (Figure 4 and Figure S6 in Supporting Information S1). In contrast, South-East of China and USA experience a reduction in the capacity of outdoor labor due to more moist heat in JJA.

Changes of monthly average capacity of outdoor labor are larger than the seasonal average changes. For instance, across three ESMs, in some locations (grid cells), the changes in the monthly average capacity of outdoor labor could reach −8.4 and +14.8% points (Figure S7 in Supporting Information S1).

### 3.1.2. Irrigation Expansion

While both CESM and MPI-ESM show an irrigation-induced reduction of annual average temperature due to increased evaporation, the models show different spatial patterns and magnitudes of local effects (Figure S9 in Supporting Information S1). For example, compared to MPI-ESM, CESM reveals a strong and consistent reduction of temperature in India and East Africa, where the annual average temperature could decrease by more than 1°C (Figure S9 in Supporting Information S1). This is likely because, in MPI-ESM, irrigation water availability is constrained by the amount of runoff and drainage, whereas, in CESM, the availability of irrigation water is unlimited. An irrigation-induced decrease of temperature indicates an evaporative cooling effect, which could potentially reduce heat stress in low latitudes. However, irrigation also causes additional humidity, which is another important factor determining thermal comfort and heat stress. For instance, a high humidity prevents the evaporation of sweat from the body. Both CESM and MPI-ESM show that the local effects of irrigation lead to an increase of relative humidity (Figure S9 in Supporting Information S1). As a result, in CESM, the evaporative cooling effect of reduced temperature is largely offset by an increase of humidity. This is indicated by substantially less pronounced absolute changes of ESI compared to the temperature response. CESM and MPI-ESM show different
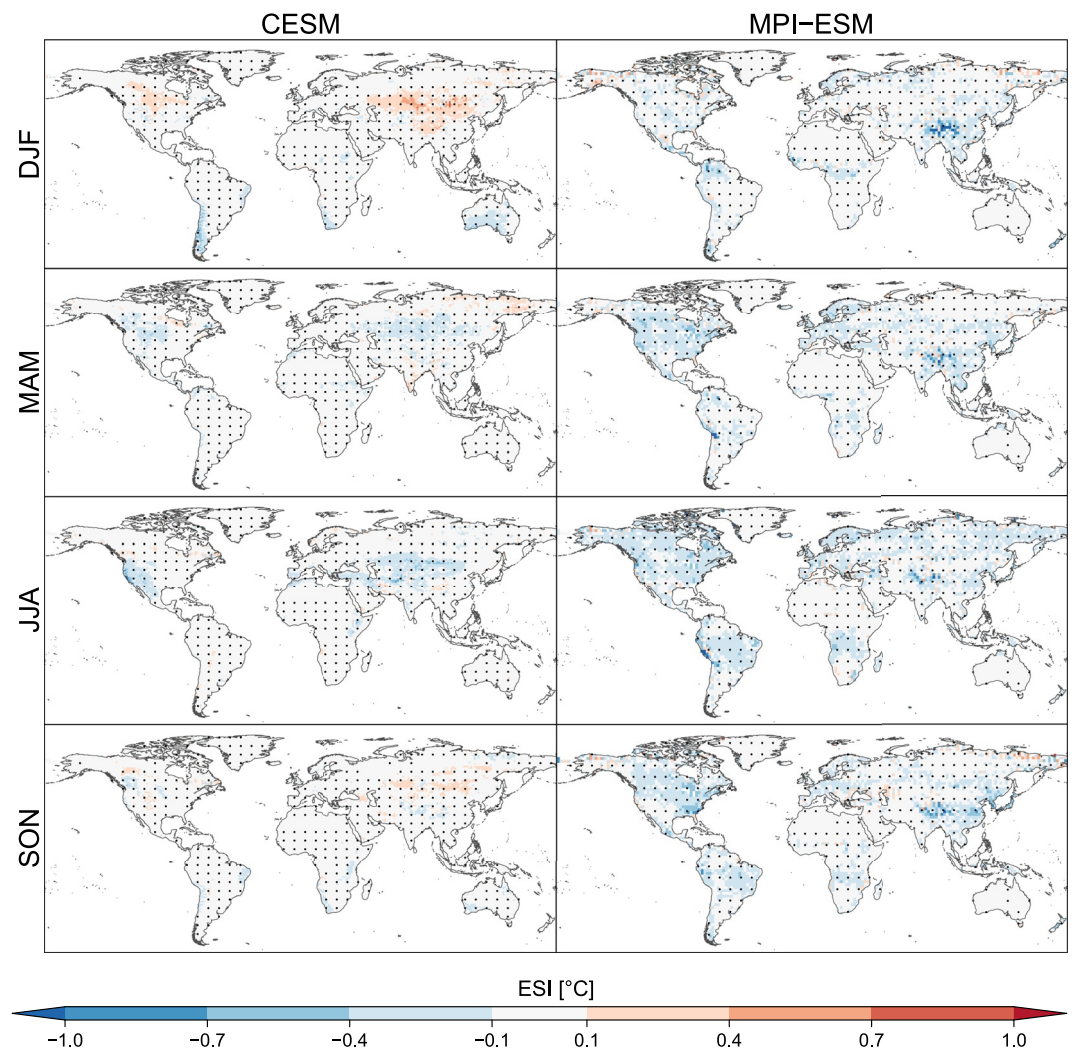
**Figure 5.** Same as Figure 2 but for the sensitivity experiment of irrigation expansion.

evaporative cooling effects. While MPI-ESM simulates a slight reduction of ESI, which is consistent with the temperature response, in CESM, irrigation expansion leads to a relatively larger increase of humidity. Relative humidity is closely correlated with temperature, while specific humidity can vary independently of temperature. In CESM, irrigation expansion also causes an increase in specific humidity (Figure S9 in Supporting Information S1). Moreover, MPI-ESM shows a larger local increase in cloud cover due to irrigation expansion compared to CESM (De Hertog et al., 2023), which could potentially explain a reduction in shortwave solar radiation. As a result, MPI-ESM has a more pronounced and widespread ESI cooling. Overall, the local effects of irrigation on moist heat stress are modest (Figures 5 and 6). The consequential impact of heat stress on the seasonal capacity of outdoor labor are also moderate in most regions, though there are some hotspots regions with relatively strong responses of labor capacity (Figure 7 and Figure S10 in Supporting Information S1). For example, CESM shows a reduction in the seasonal average capacity of outdoor labor in India in MAM. In MPI-ESM, the local effects of irrigation expansion lead to an increase in the seasonal average capacity of outdoor labor in Asia, South-East USA, and Latin America. Globally, for some locations (grid cells), the monthly average changes in the labor capacity in CESM and MPI-ESM could reach −11.1 and +7.2% points (Figure S11 in Supporting Information S1).

### 3.1.3. Afforestation

In contrast to cropland expansion, the local effects of afforestation implemented in CESM and MPI-ESM lead to a local warming in high-latitude regions due to changes in turbulent heat fluxes induced by changes in land cover (Figure 8, Figures S13 in Supporting Information S1 and Figure 9 in De Hertog et al. (2023)). In CESM, the
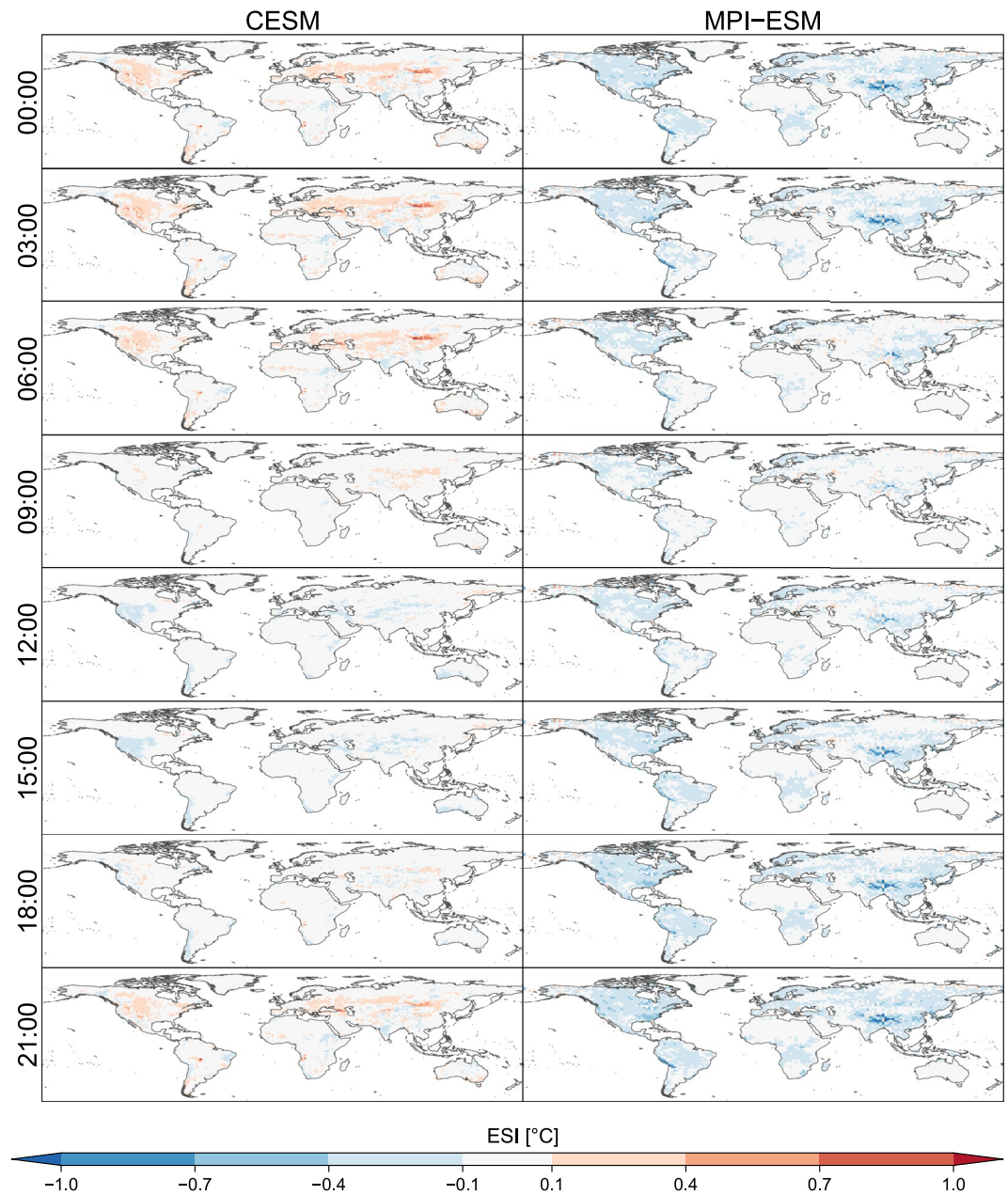
**Figure 6.** Same as Figure 3 but for the sensitivity experiment of irrigation expansion.

albedo changes completely determine the climate response, whereas in MPI-ESM, the albedo effect is less strong and thus the surface roughness and in turn the changes in turbulent heat fluxes also play an important role. The magnitude and spatial patterns of the local effects largely differ between CESM and MPI-ESM. In CESM, the local effects of afforestation are associated with cooling in some low-latitude regions due to increased evapotranspiration rates and turbulent exchange of sensible heat (Figure 9 in De Hertog et al. (2023)). The absolute changes of ESI in the tropics are slightly less pronounced than the temperature response because of changes in relative and specific humidity (Figure S13 in Supporting Information S1). CESM also shows a reduction in shortwave solar radiation. Furthermore, in CESM, afforestation leads to a local decrease (increase) of nigh-time (day-time) ESI in low latitudes, which is the reverse effect compared to cropland expansion (Figure 9). As a result of a higher day-time ESI, the seasonal average capacity of outdoor labor declines in some regions of Africa, Middle East, and West Australia (Figure 10 and Figure S14 in Supporting Information S1). In contrast, East Australia (in DJF) and Thailand (in JJA) show an increase in the capacity of outdoor labor in DJF.
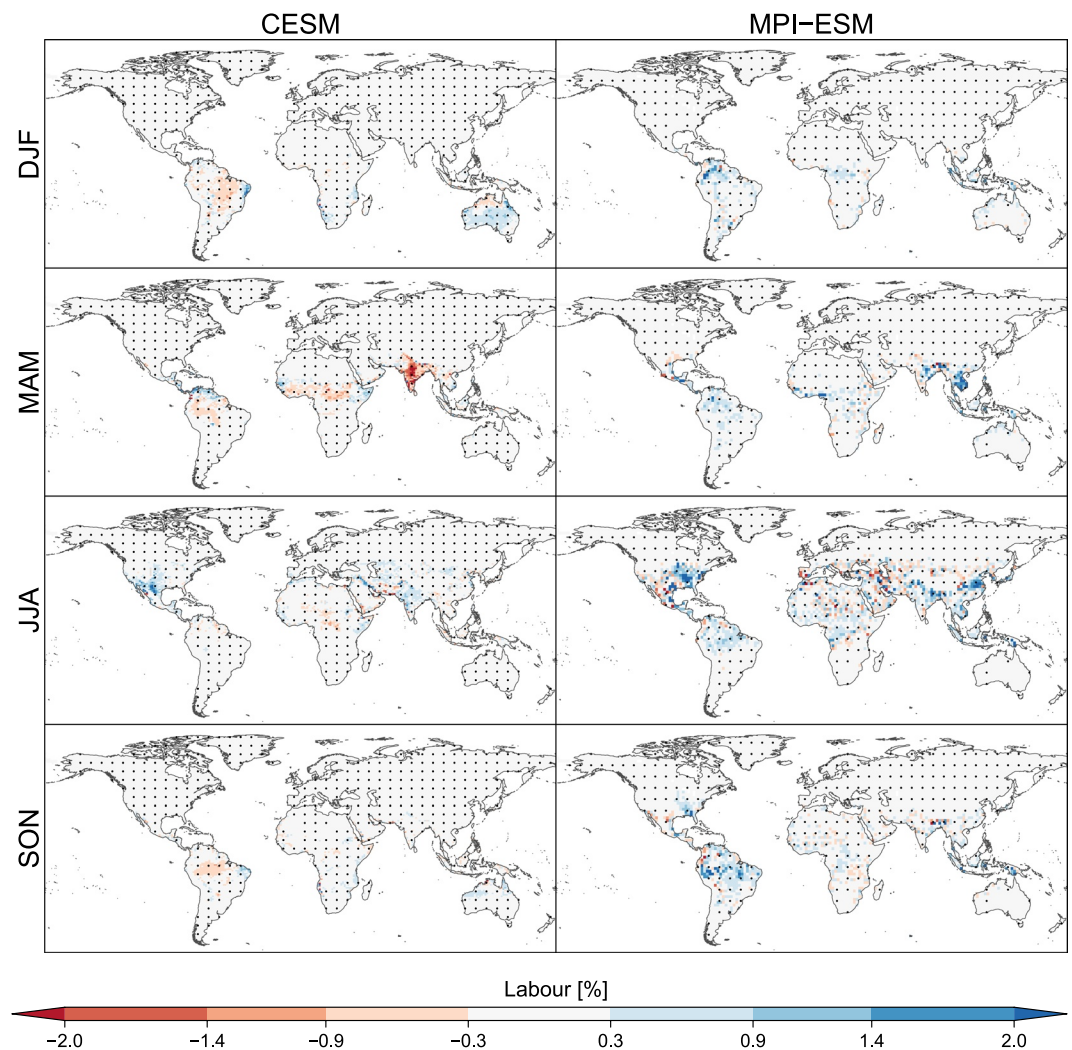
**Figure 7.** Same as Figure 4 but for the sensitivity experiment of irrigation expansion.

Similar to CESM, afforestation causes an increase in annual average temperature and a reduction in shortwave solar radiation in high latitudes (Figure S13 in Supporting Information S1). In low latitudes, MPI-ESM shows considerably smaller responses of temperature and humidity compared CESM. Moreover, MPI-ESM reveals a different diurnal cycle variation. For example, compared to CESM, MPI-ESM shows an ESI warming in the night-time and cooling in the day-time. For MPI-ESM, the labor responses are most pronounced in JJA and mixed in terms of the size of local effects (Figure 10). For example, the local effects of afforestation results in an increase in the capacity of outdoor labor in India, East and South-East Asia, and South-East USA during JJA, whereas some regions of Africa and Middle East experience a reduction of outdoor labor capacity. In EC-Earth, compared to CESM and MPI-ESM, the local effects of afforestation induce a smaller and less widespread impact on moist heat and labor capacity in most regions. Some countries of Africa, such as Sudan and Chad, South-East of China, and USA experience an increase in the seasonal average capacity of outdoor labor due to less moist heat.

Overall, across three ESMs, in some locations (grid cells), the changes in the monthly average capacity of outdoor labor range from −13.6 to +14.8% points (Figure S15 in Supporting Information S1).

### 3.1.4. Indoor Versus Outdoor Labor

Above, we presented and discussed the LCLMC-induced impacts on the capacity of outdoor labor. To investigate the impact on indoor labor (i.e., outdoor in shade, shielded from direct solar radiation), we calculated the capacity
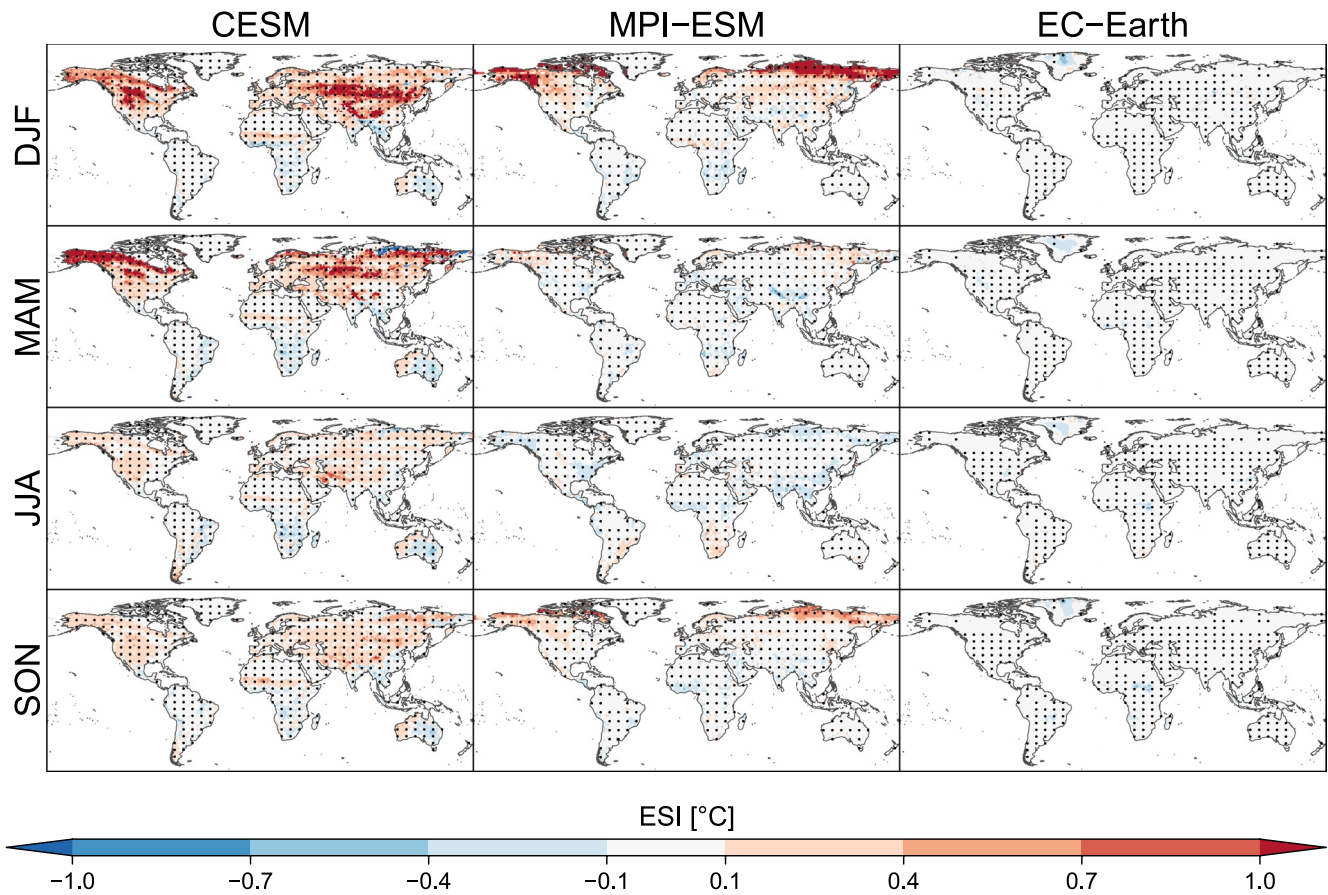
**Figure 8.** Same as Figure 2 but for the sensitivity experiment of afforestation.

of indoor labor based on the WBGT-indoors, which require only the data on temperature and relative humidity without solar radiation (Section 2.2). When comparing the responses of outdoor and indoor labor, we find that the changes in the capacity of indoor labor are substantially less pronounced (Figures S8, S12, S16 in Supporting Information S1). The differences in the responses of indoor and outdoor labor capacity are especially apparent for the sensitivity experiment of cropland expansion. For example, for CESM and EC-Earth, the local effects of cropland expansion cause a substantially smaller impact on the capacity of indoor labor in the Amazon and especially Congo regions compared to the response of outdoor labor (Figure S8 in Supporting Information S1). For example, for the Congo region, changes in indoor labor capacity due to cropland expansion do not exceed 1% point.

### 3.2. Non-Local Effects

### 3.2.1. Cropland Expansion

Overall, the non-local effects of cropland expansion are inconsistent across the ESMs. In CESM, the non-local effects of cropland expansion cause a strong global ESI cooling (Figure 11), which is associated with increases in the vegetation albedo and snow albedo feedback (Appendix D in De Hertog et al. (2023)). In other words, the local albedo changes cause the non-local ESI cooling through atmospheric circulation. Due to a lower temperature, the snow persists longer over open cropland than in afforested areas. Moreover, the increased albedo effect is stronger in a snow-covered cropland or bare soil area than for snow covered afforested area (Davin & Noblet-Ducoudré, 2010). The nonlocal global cooling leads to a relatively strong increase in the capacity of outdoor labor in the tropics, especially in West Africa, Middle East, and North Australia (Figure 12).

In contrast to CESM, in MPI-ESM, the non-local effects of cropland expansion cause an increase of ESI in the polar and temperate zone (Figure 11) because other biogeophysical effects (i.e., changes in cloud cover) compensate a relatively small albedo effect (De Hertog et al., 2023). However, for most high-latitude regions, the non-local effects are inconsistent across five 30-year time slices of MPI-ESM. Some low-latitude regions,
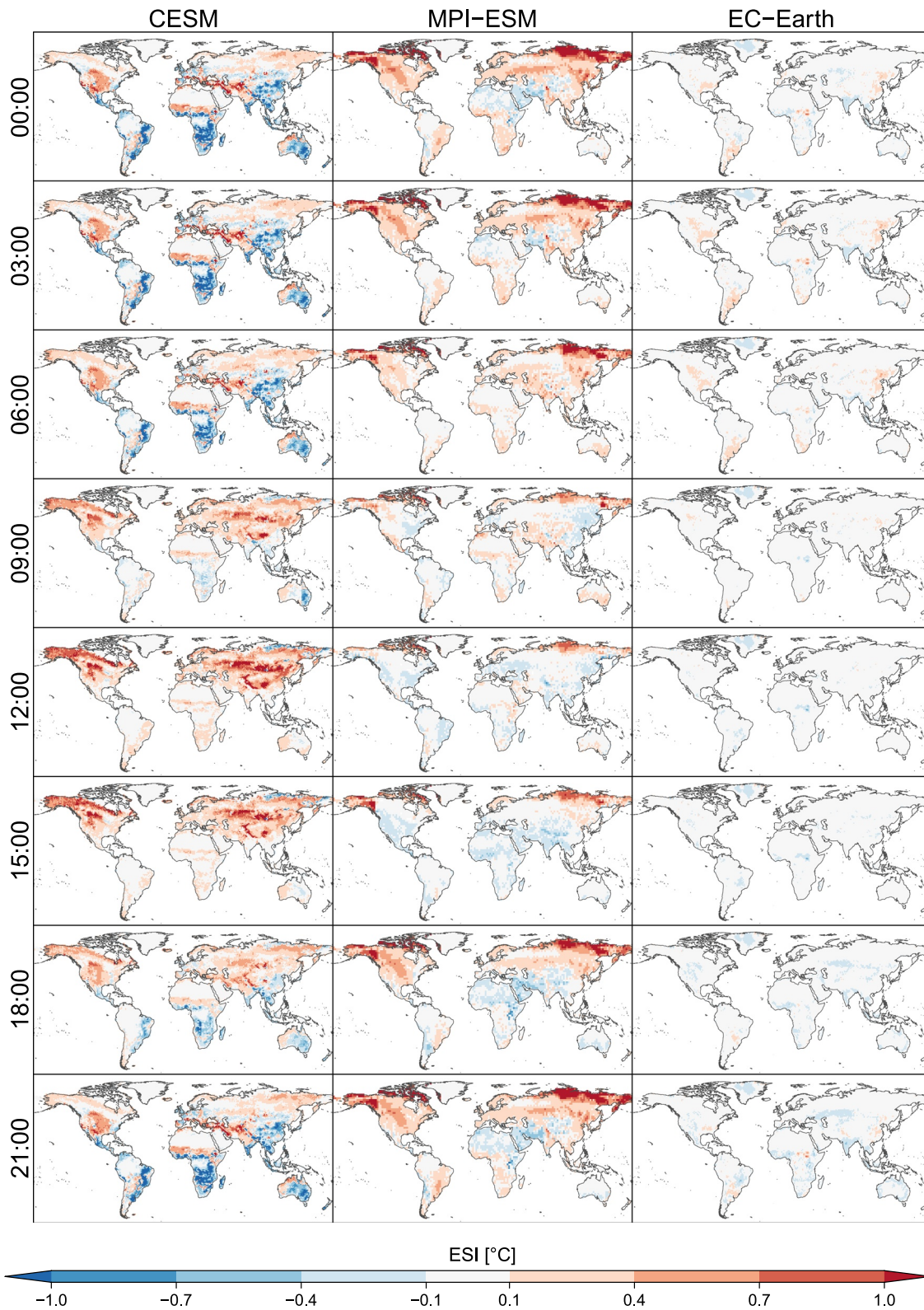
**Figure 9.** Same as Figure 3 but for the sensitivity experiment of afforestation.
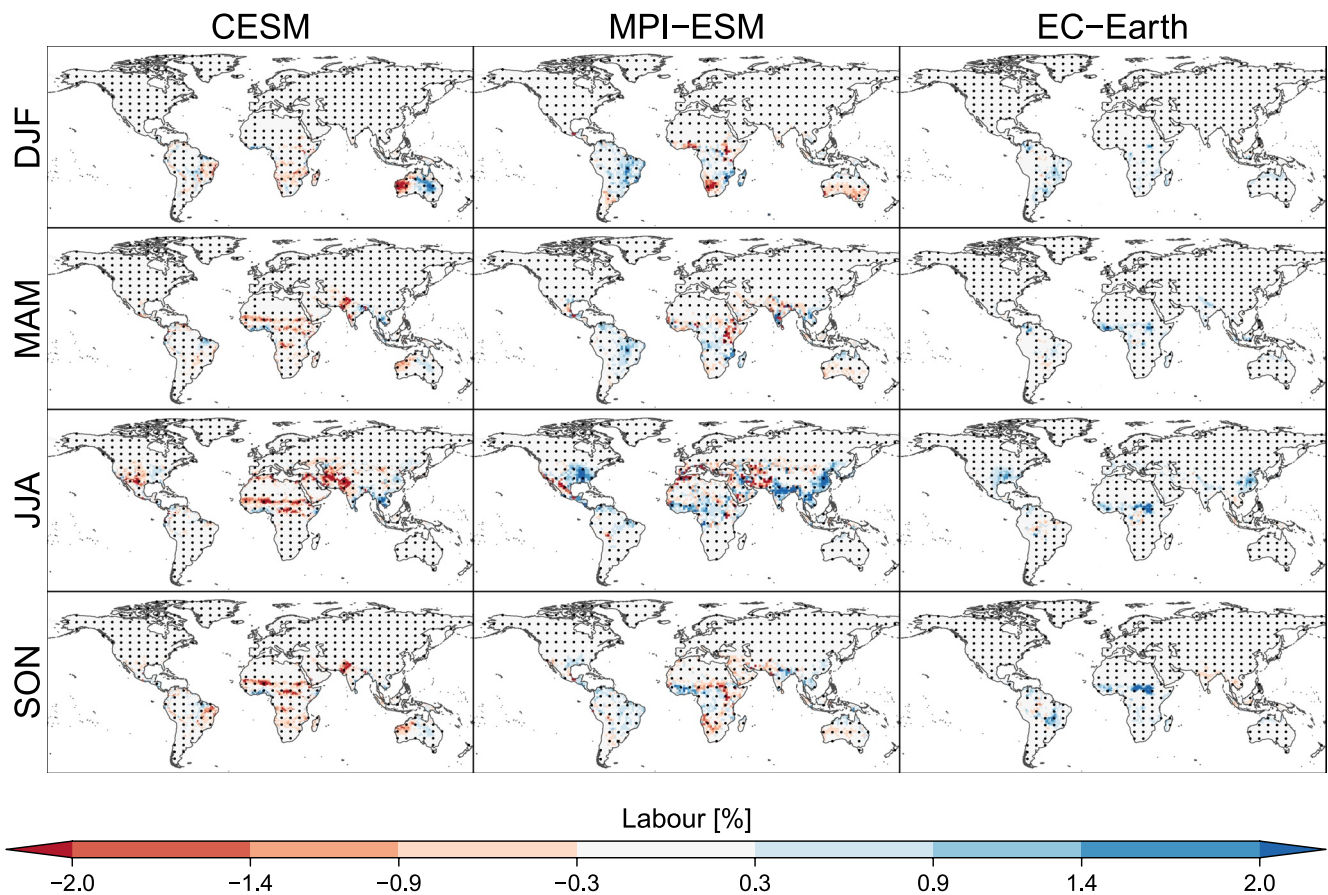
**Figure 10.** Same as Figure 4 but for the sensitivity experiment of afforestation.

such as the Amazon, Central Africa, South-East Asia, and Australia, experience an ESI cooling, which leads to a moderate increase in the capacity of outdoor labor (Figure 12).

Similar to CESM, in EC-Earth, the non-local effects of cropland expansion result in a reduction of ESI in the boreal regions, which is, however, less spatially widespread and less pronounced compared to CESM. Furthermore, in contrast to CESM and MPI-ESM, in EC-Earth, the non-local effects of cropland expansion induce an increase in the annual average ESI in Africa, Middle East, and Amazon area. In EC-Earth, a local warming induced by cropland expansion in the tropics is amplified by atmospheric circulation processes. As a result of ESI warming, the capacity of outdoor labor decreases in North and Central Africa, Middle East, South-East Asia, and especially the Amazon region.

### 3.2.2. Irrigation Expansion

In CESM and EC-Earth, the non-local effects of irrigation on moist heat are small and largely inconsistent between these two ESMs. Moreover, the robustness across five 30-year time slices is generally lower than for the local effects, potentially because of the interannual variability of atmospheric circulation patterns. Both models indicate a modest increase in moist heat in the Saharan and Sahel regions, leading to a lower capacity of outdoor labor (Figures 11 and 12). CESM also shows a small decrease of ESI in high latitudes (e.g., North America). By contrast, in MPI-ESM, the non-local effects of irrigation expansion result in a strong global decrease of ESI because of a non-local increase in cloud cover. As a result of a global ESI cooling, the capacity of outdoor labor increases in the tropics and especially in South-West USA (Figure 12). For most regions except the USA, the changes in the annual average capacity of outdoor labor do not exceed 2% points.

### 3.2.3. Afforestation

Afforestation-induced albedo decreases lead to a local warming in the boreal region. The non-local effects of afforestation results in an ESI warming in the tropics through atmospheric circulation, which transports a
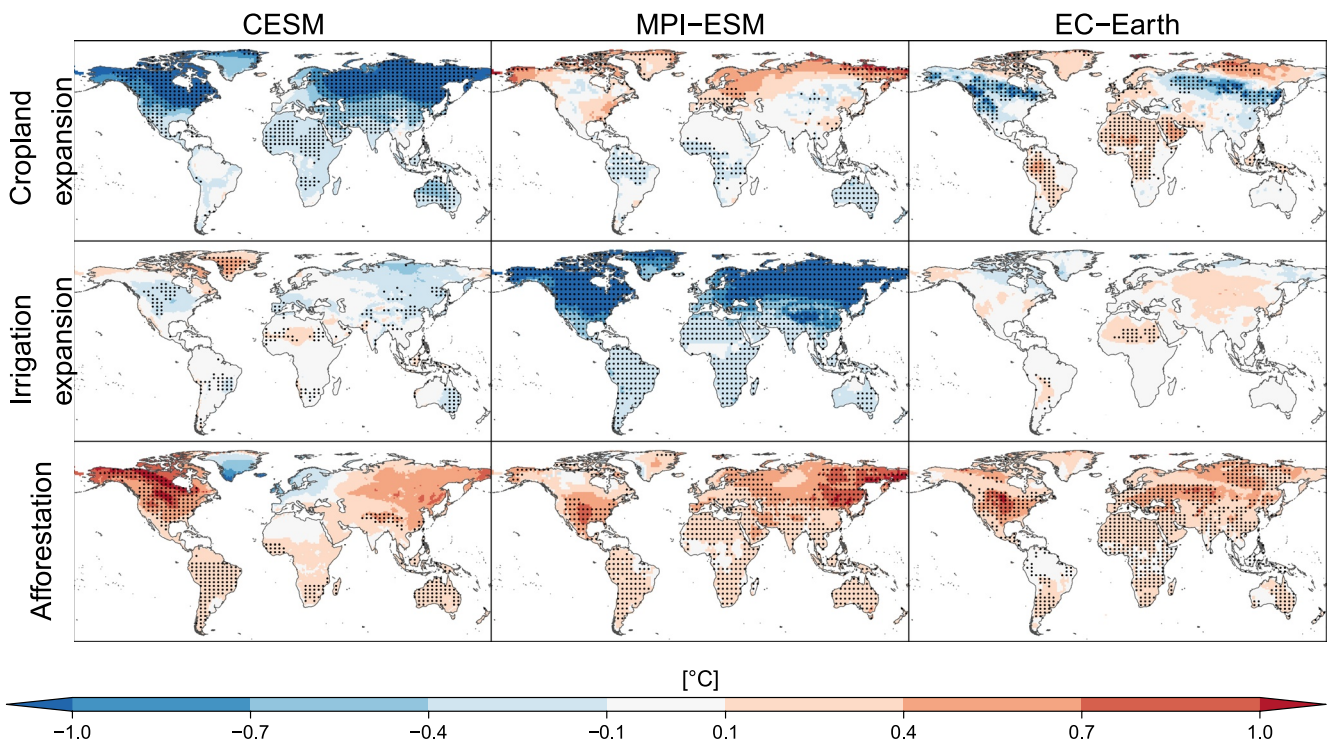
**Figure 11.** Ensemble-mean absolute changes (in Celsius) of the annual average Environmental Stress Index (ESI) for a 7 a.m. to 7 p.m. workday, which result from the non-local effects of cropland expansion, irrigation expansion, and afforestation. The dots indicate the consistency in terms of the sign of local effects across five 30-year time slices.



**Figure 12.** Ensemble-mean absolute changes (in percentage points) of the annual average labor capacity of high work-intensive jobs in outdoors for a 7 a.m. to 7 p.m. workday, which result from the non-local effects of cropland expansion, irrigation expansion, and afforestation. The dots indicate the consistency in terms of the sign of local effects across five 30-year time slices.
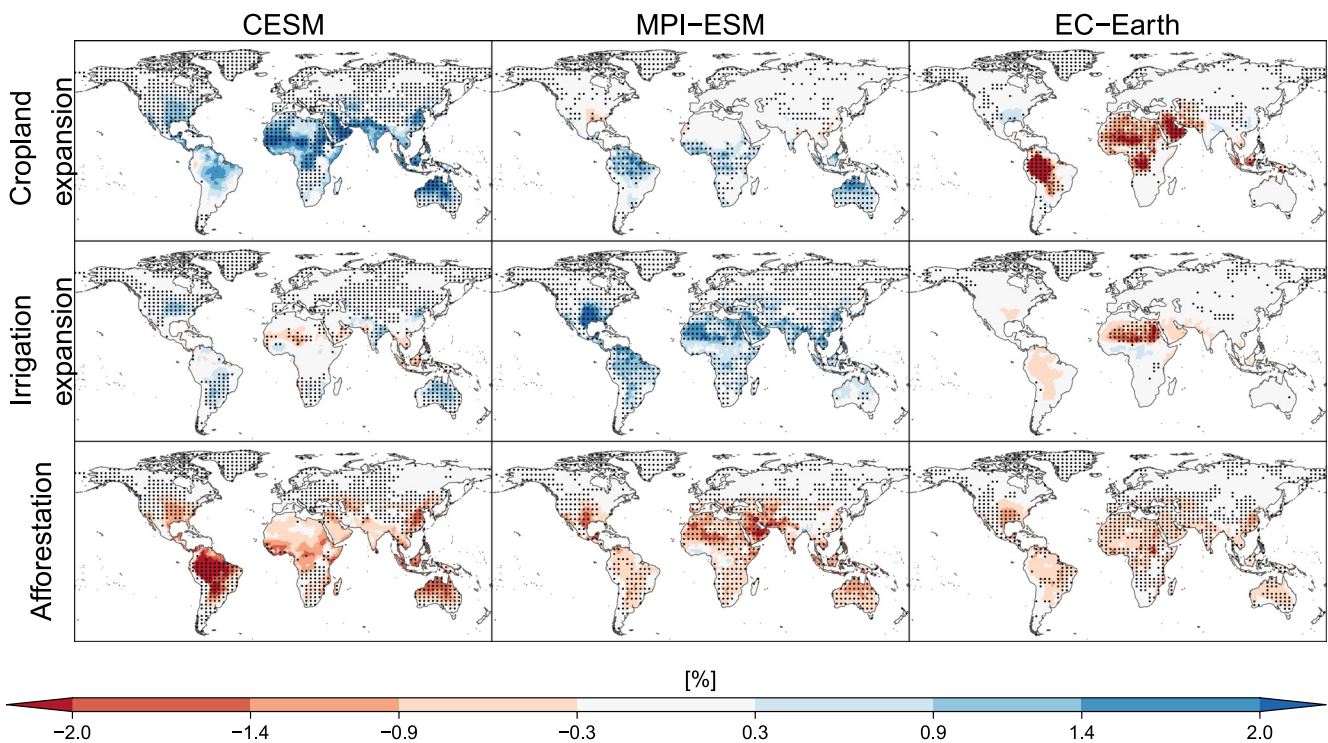
warmer air from high latitudes. The magnitude and spatial patterns of warming strongly differ across the ESMs (Figure 11). For instance, in CESM, the non-local effects are largely inconsistent across five 30-year time slices for Eurasia and a large part of Africa, while North America is shown to experience a consistent increase of ESI. In MPI-ESM, the ESI warming is especially strong in China, USA, and Russian Far East. As a result of increased heat stress, the capacity of outdoor labor declines in the tropics (Figure 12). In CESM, the reductions in the capacity of outdoor labor are especially strong in Latin America and North Australia, while, in MPI-ESM, the decline of labor capacity is most pronounced in Middle East. In EC-Earth, the heat-induced reductions of the annual average capacity of outdoor labor in the tropics do not exceed 1% point.

## 4. Discussion

Most existing epidemiological studies on heat-related mortality and morbidity use only ambient temperature as the main climatic explanatory variable to assess health impacts. More sophisticated heat indexes, which include humidity and other climate variables, are rarely used (Heo et al., 2019; Ma et al., 2018). Results of our analysis show that humidity is an important factor when analyzing the biogeophysical effects of irrigation expansion on moist heat and labor capacity. We found that the irrigation-induced local decline in air temperature could be opposed by a local increase in humidity. In CESM, irrigation expansion even leads to a reduction of labor capacity because of more moist heat (Figure 7), whereas, in MPI-ESM, the local effects are dominated by an increase of labor capacity due to an ESI cooling. Observation-based studies found that irrigation could lead to an increase of moist heat in India (Guo et al., 2022; Mishra et al., 2020). However, they use a different index to measure moist heat and investigate the effects of current irrigation while our idealized sensitivity experiment applies 0% and 100% irrigation. Therefore, the results of our analysis are not directly comparable with Mishra et al. (2020). For cropland expansion and afforestation, we also found that the absolute changes of ESI are less pronounced compared to the temperature responses due to concomitant changes of humidity.

Furthermore, we found several sources of disagreement across the ESMs which hinder from drawing robust conclusions. One aspect is the divergent responses of moist heat during day-time and night-time. For instance, CESM and EC-Earth show that cropland expansion causes an increase in moist heat during night-time and a decrease during day-time, while MPI-ESM has rather a reverse response. It should be noted that MPI-ESM model output data have a relatively coarse temporal resolution (6-hourly), which affects the estimates of labor responses for a 7 a.m. to 7 p.m. workday. In both CESM and EC-Earth, cropland expansion in low latitudes induces a substantially smaller increase in temperature during day-time compared to night-time. Moreover, the increase in day-time temperature in low latitudes is counteracted by a reduction in humidity, the combination of both resulting in a decrease in ESI. Due to a lack of data needed for an entire energy balance decomposition, it is difficult to fully explain the diurnal cycle variation of temperature in our ESM simulations. Overall, in MPI-ESM, the spatial distribution of surface heat fluxes agrees well with temperature responses (except for the high northern latitudes), which implies that the diurnal variation of temperature responses can be largely explained by variations in surface heat fluxes. Generally, an increase in sensible heat flux or a decrease in latent heat flux causes an increase in near-surface temperature and vice versa (Figure S17 in Supporting Information S1). However, in CESM and EC-Earth, changes in sensible and latent heat fluxes do not agree with temperature response, meaning that other variables play a determining role. For example, in CESM, the largest reduction in latent heat flux due to cropland expansion occurs in the afternoon; however, the temperature increase is substantially smaller in magnitude and spatial coverage in day-time compared to night-time. Potentially, albedo changes might explain a smaller temperature response in day-time as especially an albedo increase due to cropland expansion leads to a higher fraction of reflected incoming solar radiation and thus less warming. In CESM and MPI-ESM, cropland expansion results in a stronger incoming solar radiation; however, both sensible and latent heat fluxes decrease between 09:00 and 15:00. This indicates that roughness reductions due to cropland expansion might also be an important deriver of temperature responses by reducing both sensible and latent heat fluxes. In both CESM and EC-Earth, the diurnal cycle variation of temperature responses is rather counter-intuitive, while observations support the results of MPI-ESM (Figure S18–S19 in Supporting Information S1). Observation-based studies show that deforestation (afforestation) leads to cooling (warming) during night-time and warming (cooling) during daytime, which contradicts the results of CESM and EC-Earth (Alkama & Cescatti, 2016; Duveiller et al., 2018; Lee et al., 2011). This is especially true for surface temperature; however, changes of near-surface climate variables (relevant for the calculation of ESI and other moist heat indices) are subject to more uncertainty and inconsistencies across models. For instance, results from the applied ESMs show that the response of near-surface temperature to

LCLMC is found to be substantially less pronounced and less consistent across the models compared to surface temperature (De Hertog et al., 2023; Winckler et al., 2019).

Moreover, LCLMC-induced effects on cloud cover and albedo changes are inconsistent and highly uncertain across the ESMs. For instance, CESM shows a stronger albedo response compared to MPI-ESM. Overall, future research on this topic would strongly benefit from more observation-based studies as well as model development to better understand how LCLMC-induced biogeophysical effects will affect the diurnal variation of temperature, humidity, and moist heat, but also how changes in surface climate responses transfer into near-surface responses.

The nonlocal effects of LCLMC are found to have a more pronounced and spatially wide-spread impact on moist heat and labor capacity. Yet, the magnitude and spatial patterns of non-local effects, which are driven by atmospheric circulation processes, are highly inconsistent across the ESMs. In contrast to local effects, the non-local effects are scenario-dependent and therefore, for more realistic LCLMC scenarios, the non-local effects are expected to be smaller.

There are several limitations and caveats to this analysis. The main methodological challenges and limitations to the implementation of the conducted sensitivity experiments are well described in (De Hertog et al., 2023). To summarize the main limitations, the checkerboard approach introduces an interpolation error (up to 0.3 K for temperature); and, due to differences in land cover changes and modeling of biogeophysical processes in the ESMs, the conducted simulations are not perfectly consistent and comparable across the ESMs. The sensitivity experiments are highly idealized, while less extreme and more policy feasible LCLMC would lead to less pronounced impacts than estimated, especially for the non-local effects. In addition, specifically for the sensitivity experiment on irrigation expansion, the implementation of irrigation in the ESMs does not distinguish between different types of irrigation methods, which could have different biogeophysical effects (Yao et al., 2022). For example, drip irrigation will likely have a smaller effect on the climate compared to sprinkler or flood irrigation. Investigating the biogeophysical effects of different types of irrigation systems is a relevant avenue for future research. Also, the duration of irrigation-induced effects is uncertain, depending on the type of irrigation and climatic and soil conditions. Furthermore, the effects of LCLMC have been identified for the present-day climatic conditions, while the magnitude of local and non-local LCLMC-induced effects could differ under future high warming scenarios. For example, Winckler et al. (2017b) showed that deforestation-induced biogeophysical effects on local temperatures increase substantially under global warming, even reaching, in some scenarios, a strength similar to that of the present-day LCLMC effect itself. While future climate change could exacerbate LCLMC effects on climate, also the relationship between climate change and labor capacity itself could change. Due to nonlinearities in the exposure-response relationship between heat stress and labor capacity (Kjellstrom et al., 2018), the effects of LCLMC are expected to lead to more pronounced heat stress impacts under future high warming scenarios. In our analysis, we use high-end exposure-response functions (i.e., NIOSH recommendations), so the estimated impacts on labor capacity can be considered as upper bounds. Furthermore, our analysis focuses solely on the adverse heat stress impacts on labor capacity, while cold-related impacts on labor capacity are not included. A more comprehensive analysis on the LCLMC-induced climate effects on health, productivity and capacity of labor is an important avenue for future research.

## 5. Conclusions

There has been little evidence on how LCLMC would affect human heat stress and labor capacity. Previous studies lack a comprehensive perspective that impedes their comparability, which calls for a global, multi-model, multi-LCLMC approach as pursued in this study. Our analysis is based on results from three idealized sensitivity experiments considering (a) cropland expansion, (b) irrigation expansion, and (c) afforestation, which were conducted by three ESMs, namely CESM, MPI-ESM, and EC-Earth. We found that the local LCLMC-induced effects on climate are substantial but differ in space, magnitude, and sign across the ESMs. In CESM, the local effects of irrigation expansion result in a higher humidity, which largely diminishes the concomitant cooling effect of reduced temperature. Similarly, for cropland expansion, a reduction of humidity largely diminishes warming due to increased temperature in low latitudes, so the absolute changes of ESI are substantially smaller than the temperature response. Moreover, CESM and EC-Earth show that cropland expansion causes a local increase (decrease) of ESI in the night-time (day-time), which leads to a higher labor capacity in the Amazon and Congo regions due to less moist heat. In contrast, MPI-ESM, for which the response of the diurnal cycle of near-surface temperature agrees better with observations than for CESM and EC-Earth, tends to show a reversed local effect

of cropland expansion on moist heat during night- and day-time. The local effects of cropland expansion also differ by season and are inconsistent across the ESMs for some regions. For afforestation, the local effects on moist heat and labor capacity are mixed. Overall, the local LCLMC-induced effects could lead to non-negligible impacts on labor capacity in low-latitude regions during the warmest seasons. We found that, in some locations, the LCLMC-induced changes in the monthly average capacity of outdoor labor across all grid cells within a region could reach −14 and +15% points relative to the levels of labor capacity under current climate conditions and land use. Our results thus highlight that these effects may be of real significance locally but are at the same time uncertain and would benefit from more observational studies as well as from further model evaluation and development.

Finally, we found that the non-local effects of LCLMC could also affect the labor capacity through changes in heat stress. These effects are substantial but differ across the ESMs in our idealized experiments. The non-local effects are scenario-dependent, and these would therefore be substantially smaller in more policy feasible LCLMC scenarios. Despite the mentioned limitations and inconsistencies across the ESMs, results of our analysis show that the LCLMC-induced impacts on human heat stress and labor capacity should be considered in LCLMC-related policies to enhance sustainable development.

## Conflict of Interest

The authors declare no conflicts of interest relevant to this study.

## Data Availability Statement

The signal-separated data analysed in this paper will be made available through the DOKU at DKRZ. https://www.wdc-climate.de/ui/entry?acronym=DKRZ_LTA_1147_ds00002.

## References

Akkermans, T., Thiery, W., & Lipzig, N. P. M. V. (2014). The regional climate impact of a realistic future deforestation scenario in the Congo Basin. *Journal of Climate*, *27*(7), 2714–2734. https://doi.org/10.1175/JCLI-D-13-00361.1

Alkama, R., & Cescatti, A. (2016). Biophysical climate impacts of recent changes in global forest cover. *Science*, *351*(6273), 600–604. https://doi.org/10.1126/science.aac8083

Alves de Oliveira, B. F., Bottino, M. J., Nobre, P., & Nobre, C. A. (2021). Deforestation and climate change are projected to increase heat stress risk in the Brazilian Amazon. *Communications Earth & Environment*, *2*, 1–8. https://doi.org/10.1038/s43247-021-00275-8

Baker, J. C. A., & Spracklen, D. V. (2019). Climate benefits of intact amazon forests and the biophysical consequences of disturbance. *Frontiers in Forest and Global Change*, *2*, 47. https://doi.org/10.3389/ffgc.2019.00047

Boysen, L. R., Brovkin, V., Pongratz, J., Lawrence, D. M., Lawrence, P., Vuichard, N., et al. (2020). Global climate response to idealized deforestation in CMIP6 models. *Biogeosciences*, *17*(22), 5615–5638. https://doi.org/10.5194/bg-17-5615-2020

Budd, G. M. (2008). Wet-bulb globe temperature (WBGT)—Its history and its limitations. *Journal of Science and Medicine in Sport, Heat Stress in Sport*, *11*(1), 20–32. https://doi.org/10.1016/j.jsams.2007.07.003

Buzan, J. R., Oleson, K., & Huber, M. (2015). Implementation and comparison of a suite of heat stress metrics within the community land model version 4.5. *Geoscientific Model Development*, *8*(2), 151–170. https://doi.org/10.5194/gmd-8-151-2015

Chen, L., & Dirmeyer, P. A. (2019). Global observed and modelled impacts of irrigation on surface temperature. *International Journal of Climatology*, *39*(5), 2587–2600. https://doi.org/10.1002/joc.5973

Danabasoglu, G., Lamarque, J.-F., Bacmeister, J., Bailey, D. A., DuVivier, A. K., Edwards, J., et al. (2020). The community Earth system model version 2 (CESM2). *Journal of Advances in Modeling Earth Systems*, *12*, e2019MS001916. https://doi.org/10.1029/2019MS001916

Davin, E. L., & Noblet-Ducoudré, N. D. (2010). Climatic impact of global-scale deforestation: Radiative versus nonradiative processes. *Journal of Climate*, *23*(1), 97–112. https://doi.org/10.1175/2009JCLI3102.1

De Hertog, S. J., Havermann, F., Vanderkelen, I., Guo, S., Luo, F., Manola, I., et al. (2023). The biogeophysical effects of idealized land cover and land management changes in Earth system models. *EGUsphere*, 1–58. https://doi.org/10.5194/egusphere-2023-253

De Vrese, P., Hagemann, S., & Claussen, M. (2016). Asian irrigation, African rain: Remote impacts of irrigation. *Geophysical Research Letters*, *43*(8), 3737–3745. https://doi.org/10.1002/2016GL068146

Döscher, R., Acosta, M., Alessandri, A., Anthoni, P., Arsouze, T., Bergman, T., et al. (2022). The EC-Earth3 Earth system model for the coupled model intercomparison project 6. *Geoscientific Model Development*, *15*(7), 2973–3020. https://doi.org/10.5194/gmd-15-2973-2022

Dunne, J. P., Stouffer, R. J., & John, J. G. (2013). Reductions in labour capacity from heat stress under climate warming. *Nature Climate Change*, *3*(6), 563–566. https://doi.org/10.1038/nclimate1827

Duveiller, G., Hooker, J., & Cescatti, A. (2018). The mark of vegetation change on Earth's surface energy balance. *Nature Communications*, *9*(1), 679. https://doi.org/10.1038/s41467-017-02810-8

Fatima, S. H., Rothmore, P., Giles, L. C., Varghese, B. M., & Bi, P. (2021). Extreme heat and occupational injuries in different climate zones: A systematic review and meta-analysis of epidemiological evidence. *Environment International*, *148*, 106384. https://doi.org/10.1016/j.envint.2021.106384

Fischer, E. M., & Knutti, R. (2013). Robust projections of combined humidity and temperature extremes. *Nature Climate Change*, *3*(2), 126–130. https://doi.org/10.1038/nclimate1682

Gasparrini, A., Guo, Y., Hashizume, M., Lavigne, E., Zanobetti, A., Schwartz, J., et al. (2015). Mortality risk attributable to high and low ambient temperature: A multicountry observational study. *Lancet London England*, *386*(9991), 369–375. https://doi.org/10.1016/S0140-6736(14)62114-0

Guo, Q., Zhou, X., Satoh, Y., & Oki, T. (2022). Irrigated cropland expansion exacerbates the urban moist heat stress in northern India. *Environmental Research Letters*, *17*(5), 054013. https://doi.org/10.1088/1748-9326/ac64b6

Heo, S., Bell, M. L., & Lee, J.-T. (2019). Comparison of health risks by heat wave definition: Applicability of wet-bulb globe temperature for heat wave criteria. *Environmental Research*, *168*, 158–170. https://doi.org/10.1016/j.envres.2018.09.032

Hurtt, G. C., Chini, L., Sahajpal, R., Frolking, S., Bodirsky, B. L., Calvin, K., et al. (2020). Harmonization of global land use change and management for the period 850–2100 (LUH2) for CMIP6. Geosci. *Model Development*, *13*(11), 5425–5464. https://doi.org/10.5194/gmd-13-5425-2020

Kjellstrom, T., Freyberg, C., Lemke, B., Otto, M., & Briggs, D. (2018). Estimating population heat exposure and impacts on working people in conjunction with climate change. *International Journal of Biometeorology*, *62*(3), 291–306. https://doi.org/10.1007/s00484-017-1407-0

Kjellstrom, T., Holmer, I., & Lemke, B. (2009). Workplace heat stress, health and productivity – An increasing challenge for low and middle-income countries during climate change. *Global Health Action*, *2*(1), 2047. https://doi.org/10.3402/gha.v2i0.2047

Kjellstrom, T., Maitre, N., Saget, C., Otto, M., & Karimova, T. (2019). Working on a warmer planet: The effect of heat stress on productivity and decent work (Report).

Kong, Q., & Huber, M. (2022). Explicit calculations of wet-bulb globe temperature compared with approximations and why it matters for labor productivity. *Earth's Future*, *10*(3), e2021EF002334. https://doi.org/10.1029/2021EF002334

Krakauer, N. Y., Cook, B. I., & Puma, M. J. (2020). Effect of irrigation on humid heat extremes. *Environmental Research Letters*, *15*(9), 094010. https://doi.org/10.1088/1748-9326/ab9ecf

Lee, X., Goulden, M. L., Hollinger, D. Y., Barr, A., Black, T. A., Bohrer, G., et al. (2011). Observed increase in local cooling effect of deforestation at higher latitudes. *Nature*, *479*(7373), 384–387. https://doi.org/10.1038/nature10588

Lejeune, Q., Davin, E. L., Guillod, B. P., & Seneviratne, S. I. (2015). Influence of Amazonian deforestation on the future evolution of regional surface fluxes, circulation, surface temperature and precipitation. *Climate Dynamics*, *44*(9–10), 2769–2786. https://doi.org/10.1007/s00382-014-2203-8

Lemke, B., & Kjellstrom, T. (2012). Calculating workplace WBGT from meteorological data: A tool for climate change assessment. *Industrial Health*, *50*(4), 267–278. https://doi.org/10.2486/indhealth.MS1352

Liljegren, J. C., Carhart, R. A., Lawday, P., Tschopp, S., & Sharp, R. (2008). Modeling the wet bulb globe temperature using standard meteorological measurements. *Journal of Occupational and Environmental Hygiene*, *5*(10), 645–655. https://doi.org/10.1080/15459620802310770

Lindeskog, M., Arneth, A., Bondeau, A., Waha, K., Seaquist, J., Olin, S., & Smith, B. (2013). Implications of accounting for land use in simulations of ecosystem carbon cycling in Africa. *Earth System Dynamics*, *4*(2), 385–407. https://doi.org/10.5194/esd-4-385-2013

Ma, C., Honda, Y., & Dang, T. N. (2018). Comparison of wet-bulb globe temperature (WBGT) and mean temperature for assessment of heat-related mortality. *Japanese Journal of Health and Human Ecology*, *84*(2), 52–72. https://doi.org/10.3861/kenko.84.2_52

Masuda, Y. J., Garg, T., Anggraeni, I., Ebi, K., Krenz, J., Game, E. T., et al. (2021). Warming from tropical deforestation reduces worker productivity in rural communities. *Nature Communications*, *12*(1), 1601. https://doi.org/10.1038/s41467-021-21779-z

Mauritsen, T., Bader, J., Becker, T., Behrens, J., Bittner, M., Brokopf, R., et al. (2019). Developments in the MPI-M Earth system model version 1.2 (MPI-ESM1.2) and its response to increasing $CO_2$. *Journal of Advances in Modeling Earth Systems*, *11*(4), 998–1038. https://doi.org/10.1029/2018MS001400

Mishra, V., Ambika, A. K., Asoka, A., Aadhar, S., Buzan, J., Kumar, R., & Huber, M. (2020). Moist heat stress extremes in India enhanced by irrigation. *Nature Geoscience*, *13*(11), 722–728. https://doi.org/10.1038/s41561-020-00650-8

Mora, C., Dousset, B., Caldwell, I. R., Powell, F. E., Geronimo, R. C., Bielecki, C. R., et al. (2017). Global risk of deadly heat. *Nature Climate Change*, *7*, 501–506. https://doi.org/10.1038/nclimate3322

Moran, D. S., & Epstein, Y. (2006). Evaluation of the environmental stress index (ESI) for hot/dry and hot/wet climates. *Industrial Health*, *44*(3), 399–403. https://doi.org/10.2486/indhealth.44.399

Moran, D. S., Pandolf, K. B., Shapiro, Y., Heled, Y., Shani, Y., Mathew, W. T., & Gonzalez, R. R. (2001). An environmental stress index (ESI) as a substitute for the wet bulb globe temperature (WBGT). *Journal of Thermal Biology International Thermal Physiology Symposium*, *26*(4–5), 427–431. https://doi.org/10.1016/S0306-4565(01)00055-9

NIOSH. (1986). Criteria for a recommended standard: Occupational exposure to hot environments.

Orlov, A., Daloz, A. S., Sillmann, J., Thiery, W., Douzal, C., Lejeune, Q., & Schleussner, C. (2021). Global economic responses to heat stress impacts on worker productivity in crop production. *Economics of Disasters and Climate Change*, *5*(3), 367–390. https://doi.org/10.1007/s41885-021-00091-6

Orlov, A., Sillmann, J., Aunan, K., Kjellstrom, T., & Aaheim, A. (2020). Economic costs of heat-induced reductions in worker productivity due to global warming. *Global Environmental Change*, *63*, 102087. https://doi.org/10.1016/j.gloenvcha.2020.102087

Parsons, K. (2014). *Human thermal environments: The effects of hot, moderate, and cold environments on human health, comfort, and performance*. CRC Press, Inc.

Parsons, L. A., Jung, J., Masuda, Y. J., Vargas Zeppetello, L. R., Wolff, N. H., Kroeger, T., et al. (2021). Tropical deforestation accelerates local warming and loss of safe outdoor working hours. *One Earth*, *4*(12), 1730–1740. https://doi.org/10.1016/j.oneear.2021.11.016

Pongratz, J., Schwingshackl, C., Bultan, S., Obermeier, W., Havermann, F., & Guo, S. (2021). Land use effects on climate: Current state, recent progress, and Emerging Topics. *Current Climate Change Reports*, *7*(4), 99–120. https://doi.org/10.1007/s40641-021-00178-y

Saeed, W., Haqiqi, I., Kong, Q., Huber, M., Buzan, J. R., Chonabayashi, S., et al. (2022). The poverty impacts of labor heat stress in West Africa under a warming climate. *Earth's Future*, *10*(11), e2022EF002777. https://doi.org/10.1029/2022EF002777

Stull, R. (2011). Wet-bulb temperature from relative humidity and air temperature. *Journal of Applied Meteorology and Climatology*, *50*(11), 2267–2269. https://doi.org/10.1175/JAMC-D-11-0143.1

Takakura, J., Fujimori, S., Takahashi, K., Hijioka, Y., Hasegawa, T., Honda, Y., & Masui, T. (2017). Cost of preventing workplace heat-related illness through worker breaks and the benefit of climate-change mitigation. *Environmental Research Letters*, *12*(6), 064010. https://doi.org/10.1088/1748-9326/aa72cc

Thiery, W., Davin, E. L., Lawrence, D. M., Hirsch, A. L., Hauser, M., & Seneviratne, S. I. (2017). Present-day irrigation mitigates heat extremes. *Journal of Geophysical Research: Atmospheres*, *122*(3), 1403–1422. https://doi.org/10.1002/2016JD025740

Thiery, W., Visser, A. J., Fischer, E. M., Hauser, M., Hirsch, A. L., Lawrence, D. M., et al. (2020). Warming of hot extremes alleviated by expanding irrigation. *Nature Communications*, *11*(1), 290. https://doi.org/10.1038/s41467-019-14075-4

Willett, K. M., & Sherwood, S. (2012). Exceedance of heat index thresholds for 15 regions under a warming climate using the wet-bulb globe temperature. *International Journal of Climatology*, *32*(2), 161–177. https://doi.org/10.1002/joc.2257

Winckler, J., Lejeune, Q., Reick, C. H., & Pongratz, J. (2019). Nonlocal effects dominate the global mean surface temperature response to the biogeophysical effects of deforestation. *Geophysical Research Letters*, *46*(2), 745–755. https://doi.org/10.1029/2018GL080211

Winckler, J., Reick, C. H., & Pongratz, J. (2017a). Robust identification of local biogeophysical effects of land-cover change in a global climate model. *Journal of Climate*, *30*(3), 1159–1176. https://doi.org/10.1175/JCLI-D-16-0067.1

Winckler, J., Reick, C. H., & Pongratz, J. (2017b). Why does the locally induced temperature response to land cover change differ across scenarios? *Geophysical Research Letters*, *44*(8), 3833–3840. https://doi.org/10.1002/2017GL072519

Yao, Y., Vanderkelen, I., Lombardozzi, D., Swenson, S., Lawrence, D., Jägermeyr, J., et al. (2022). Implementation and evaluation of irrigation techniques in the community land model. *Journal of Advances in Modeling Earth Systems*, *14*(12), e2022MS003074. https://doi.org/10.1029/2022MS003074